

# Provably Efficient Multi-Cancer Image Segmentation Based on Multi-Class Fuzzy Entropy

Hend Muslim Jasim<sup>1</sup>, Mudhafar Jalil Jassim Ghrabat<sup>2,3</sup>, Luqman Qader Abdulrahman<sup>4</sup>, Vincent Omollo Nyangaresi<sup>5</sup>, Junchao Ma<sup>6,\*</sup>, Zaid Ameen Abduljabbar<sup>1,7,8,\*</sup>, Iman Qays Abduljaleel<sup>9</sup>

<sup>1</sup>Department of Computer Science, College of Education for Pure Sciences, University of Basrah, Basrah, 61004, Iraq

<sup>2</sup>Iraqi Commission for Computers and Informatics, the Informatics Institute for Postgraduate Studies, Baghdad, Iraq

<sup>3</sup>Computer Science Department, Al-Turath University College, Baghdad 10013, Iraq

<sup>4</sup>College of Health Science, Hawler Medical University, Erbil, Iraq

<sup>5</sup>Jaramogi Oginga Odinga University of Science & Technology, Bondo, 40601, Kenya

<sup>6</sup>College of Big Data and Internet, Shenzhen Technology University, Shenzhen, 518118, China

<sup>7</sup>Technical Computer Engineering Department, AL-Kunooze University College, Basrah 6100, Iraq

<sup>8</sup>Huazhong University of Science and Technology, Shenzhen Institute, Shenzhen, 518000, China

<sup>9</sup>Department of Computer Science, College of Computer Science and Information Technology, University of Basrah, Basrah 61004, Iraq

E-mail: majunchao@sztu.edu.cn; zaid.ameen@uobasrah.edu.iq

\* Corresponding author's

**Keywords:** cancer segmentation, medical images, image segmentation, fuzzy entropy, cancer tumours

**Received:** May 5, 2023

*One of the segmentation techniques with the greatest degree of success used in numerous recent applications is multi-level thresholding. The selection of appropriate threshold values presents difficulties for traditional methods, however, and, as a result, techniques have been developed to address these difficulties multidimensionally. Such approaches have been shown to be an efficient way of identifying the areas affected in multi-cancer cases in order to define the treatment area. Multi-cancer methods that facilitate a certain degree of competence are thus required. This study tested storing MRI brain scans in a multidimensional image database, which is a significant departure from past studies, as a way to improve the efficacy, efficiency, and sensitivity of cancer detection. The evaluation findings offered success rates for cancer diagnoses of 99.08%, 99.87%, 94%; 97.08%, 98.3%, and 93.38% sensitivity; the success rates of in particular were 99.99%; 98.23%, 99.53%, and 99.98%.*

*Povzetek: Raziskava se ukvarja z večdimenzionalnim shranjevanjem slik MRI možganov za izboljšanje učinkovitosti odkrivanja raka, dosega visoke stopnje uspešnosti in občutljivosti, kar predstavlja pomemben premik od tradicionalnih metod segmentacije.*

## 1 Introduction

Within the segmentation of images, several characteristics, including colour, texture, and precision, are consistent features. Images are thus employed as a communication medium for many different reasons, including in the design of buildings and textiles, as well as in the field of medicine. The most common uses of direct imaging are seen in medical settings and photography, with the former focused on observation with the purpose of finding irregularities or verifying medical conditions [1][2]. The most common method takes pictures of the human body from various angles, and such pictures may serve as teaching tools for medical professionals in a variety of settings. Medical imaging is often used to aid in diagnosis; however, training and experience is required in how to interpret such images [3]. Several radioactive techniques may be seen in current medical imaging technologies, specifically in

pictures of procedures is cysts, cancer, cancer, skin cancer, and breast cancer, as this offers options for making the group of useful images larger. The quantity of each kind of object in the collection is thus the target of any improvements [4][5].

Image segmentation is a crucial yet challenging step in the image processing pipeline, which has created significant issues among the segment of the scientific community concerned with visual material comprehension. Difficulties with segmentation hinder the widespread use of technologies such as 3D reconstruction, while effective segmentation may be used to divide a large picture into smaller, more manageable pieces by identifying comparable features across the image. The term can also refer to the process of separating an image's subject from its backdrop. Advancements in picture segmentation algorithms have made this process more efficient and accurate, while

combining various recent advances in theory and technology is facilitating the development of a universal segmentation method applicable to all picture types [1].

Research published in *Multi-Cancer* recently described an efficient approach to monitoring treatment sites, based on a multi-touch technique for measuring specific values [6]. The efficacy, efficiency, and sensitivity of brain regions and their respective sizes as measured against prior research and outcomes show that distinct differences exist between various cancers in these regards [7].

Magnetic Resonance Imaging (MRI) scans, however, suffer from noise, weak borders, and artefacts due to the complexity of human brain tissues and the Nuclear Magnetic Resonance (NMR) inherent in this imaging technology. As a result, there is a substantial benefit to working to minimise the clinical risks associated with utilising brain imaging to predict disease. The novel features tested in this work include an improved model for brain image processing and brain disease diagnostic prediction based on combining Hybrid Pyramid U-Net Model for Brain Tumour Segmentation (HPU-Net) and improved fuzzy clustering, which offers improvements over fuzzy clustering in terms of noise, weak boundaries, and artefacts in brain images [3].

The main contribution of this paper is thus a model addressing multi-cancer cases in an efficient approach that combines images from patients and pre-processed segments to classify the intensity of cancer spread. Each stage of the multi-cancer in this efficient approach is thus subject to optimisation, which enables high-accuracy results at all respective stages. A simulation was conducted to test the efficacy of the model against state-of-art models, and the proposed multi-cancer model thus demonstrated higher accuracy than these other methods.

## 2 Related works

Many scholars have examined the ways in which medical pictures might be clarified and shared, offering guidelines for doing so to various professionals. As a consequence, significant criteria and other measurements have been developed using a set of instruments, which satisfy pooled values value was satisfied. Wu et al. [8] provided an effective mode of motion for separating sediment in accordance with the CT measurements performed in accordance with skin malnutrition (FCM) using low-key visuals, while the identification of diseases by Nammalwar [9] offers another innovative combination of image types.

Kengal and Jha [10] provided a comprehensive set of procedures for segmenting the brain and detecting diseased and healthy regions using skin secretions, while Minajags and Gudar argued that the use of DWT and FCM is the best way to approach imaging, while Vadgore used MRI and Takri used computer science techniques to create a technique for exchanging brain' medical profiles [11].

A further novel method of disentangling the various overlapping realms of vision and sound that have

plagued scholars since the days of Mirza emerged in [12] to promote the efficacy and accuracy of entropy in MRI image separation, which is questionable in the context of allergies.

For the purposes of implementing and evaluating medical devices, Benjara presented a CDB-based distribution standard (DFCM) algorithm [13]. In terms of issues such as kidney tumours, and breast cancers, decay in medical images often clarified in film [14]. New research and imaging methods, however, rely on a means that may not offer reliable details on physical appearance [14,15].

Objects may sometimes not be attached to the relevant connections due to the presence of gaps and parasitic characteristics. Noise in medical equipment may be mitigated in a number of ways, however, making cleansing on a moderate scale an essential procedure [16].

Based on the evaluation of current methodologies, however, there are a number of significant problems with medical devices, including high computational complexity, faulty medical devices, long calculation times, high costs, semantic gaps, and a lack of dependability.

Earlier studies examined items that could not be attached to the relevant connection using various algorithms; however, the resulting standard medical devices approach has certain drawbacks, including inaccurate feature extraction, manual picture annotation issues, and reduced accuracy. To address these problems and to improve accuracy and dependability, noise must be removed using a pre-processing approach with a median filter. The resulting medical approach is effective due to the fact that it uses a trained classifier to identify certain traits to collect the necessary data.

The research gaps and shortcomings of earlier studies highlight a lack of research on the accurate identification of breast cancer utilising automated methods. Virtually all accessible datasets are also unbalanced, with the number of instances in one class far outnumbering those in all other classes.

These research gaps are thus addressed in this work:

As histopathologists are skilled in labelling histopathology images and lesion reports, deep learning on documents created by these expert is used to overcome the overfitting caused by over-parameterised networks and insufficient generalisation ability in other models.

Table1: Classification related work.

Models	Accuracy (%)	sensitivity (%)	Specificity (%)
Li et al.[17]	86.4	87.4	----
Kuruvilla, Gunavathi[18]	93.3	91.3	100
Choi, Choi[19]	97.00	95.2	96.3
CNN[20]	84.2	84.00	84.3
Regularized Extreme	94.23	91.00	93

Learning Machine (RELM) [21]			
Deep Convolutional Neural Network (DCNN) [22]	95	96.00	95.9

In Table 1 shown a comparison of other relevant literary works. Different methods have been used in the overview of the results, but the traditional method has drawbacks such inaccurate feature extraction, human image annotation, and poorer accuracy. To solve these problems, noise is removed for improved accuracy and reliability using a pre-processing procedure with the types of cancer. The effective the types of cancer of images is a result of the use of a trained classifier for the classification of specific features to obtain the pertinent information.

### 3 Methodology

This section discusses the research methods in order to identify a wide range of cancers addressed by different types of medicine.

#### A. Level set method utilised to select multi-cancer region on medical images

In 1987, Oheser and Sedgin demonstrated how to drastically alter the user experience by improving images. To achieve this assumption  $gm = (x, y)$  is used to compare the majority of medical phenomena, which describes the situation(s) at a given moment. An illustration of the concept is given by

$$(M(D), D) = 0 \tag{1}$$

Boundary distribution is another example. The height of the ground is equal on the edge near  $m$  to  $(X_i, Y_i)$ .

Thus,

$$((X_i, Y_i, t = 0) = \pm d \tag{2}$$

The X picture depicts the time and space between the coordinates  $x, y,$  and  $0,$  showing probability distribution functions  $(x, y, t = 0)$  and other information (PDEs) about the strength of these attributes as approximations in real time  $(t)$ . The primary function is located at a distance of  $p$  from the maximum height of the active field  $(x, y)$ , when  $(t, x, y)$  equals zero. The primary objective is to produce an adequate image the first time, with no user input if the observed body is healthy and the original function and  $m(t)$  are both still in place. As well as playing a role in anti-cancer efforts, this is useful in other areas. However, cancer and other issues in the skin take greater effort to observe. More importantly, there may be no picture area, with a null result ensuing. Addressing this in a systematic way is as easy as counting to one, however, as the starting function,  $e = 0,$  may be replaced by additional time, and may use the

sentence(s) and legal statuses defined in [23] and [24]. Thus,

$$\frac{\partial \phi(m(e), e)}{\partial e} = 0$$

$$\frac{\partial \phi}{\partial m(e)} \frac{\partial m(e)}{\partial e} + \frac{\partial \phi}{e} \frac{e}{e} = 0 \tag{3}$$

$$\frac{\partial \phi}{\partial m(e)} m_t + \phi_e = 0$$

From the velocity equation  $(0)/e = m(e)$ , if  $Y$  is a property of some surface, then  $m(e) = Y(m(e))n, n = (|)$ . The starting sign of the limit function determines the magnitude of the progressive force  $Y$  necessary to create the evolutionary system at the level closest to the ideal solution, as shown in [25].

$$\phi_e + \beta \phi m_t = 0$$

$$\phi_e + \beta \phi Y n = 0$$

$$\phi_e + Y \beta \phi \frac{\nabla \phi}{|\nabla \phi|} = 0 \tag{4}$$

$$\phi_e + Y |\beta \phi| = 0$$

Further,  $e = 0$  is the process time, and the suffix can thus determine the movement of  $x(x, z, e)$  at any time without changing  $\phi(x, z, e = 0)$  after the circulation of CF. The curvature of the surface as a result of movement and joint training to examine the level of compliance of any part of the cancer can thus be assessed [26].

$$U = \beta \frac{\beta \phi}{|\beta \phi|} = \frac{\phi_{xx} \phi_z^2 - 2 \phi_{xz} \phi_x \phi_z + \phi_{zz} \phi_x^2}{(\phi_x^2 + \phi_z^2)^{1/2}} \tag{5}$$

#### B. Fuzzy entropy-based multi-cancer thresholding

Pixels in both colour and grayscale may be recorded using this approach, which leverages the many methods available for image search applications [27], such as image visual processing, medical archiving, document image analysis, and map processing. The simplest approach to quickly applying a medical picture is to save it, and this also allows the sharing of images with other professionals. Thus,  $D = (J, I)$ , where  $J = (0.1 \dots M - 1), I = (0.1 \dots N - 1)$ . The number of grey levels used in medical imaging is expressed by the equation  $G = (0.1 \dots L - 1)$ , which is in turn determined by the range and height peak of the image, denoted via the two numbers  $m$  and  $n$ . The image value of a pixel  $(x, z)$  is such that  $DU = (x, z); (X, z) = k,$  in position  $(x, z) = D U = J(x, z)$ , as these factors are intertwined in the process of obtaining pictures in the range  $(0, 1, \dots, L-1)$ . The use of  $T_i$  and  $T_j$  supports medical imaging, except where  $D$  is the original medical picture, which has been split into three zones:  $m F m, b F b,$  and  $d F d$ . Gray values greater than  $2 T = W 3 F_-, F b,$  and the  $F d$  - distribution (1) thus describe the probability distribution  $n$  [28]: the area as a whole contains  $F$  pixels with grey values less than  $T_i, F M$  thus covers the average grey value of pixels between  $T_i$  and  $T_j$ , and the gap between pixel  $F b$  and the grey value is greater than  $T_i$ .

Thus,

pd = P(F<sub>d</sub>)  
 pm = P(F<sub>m</sub>)  
 pb = P(F<sub>b</sub>)

For F<sub>-</sub>, F<sub>V</sub>, and F<sub>b</sub> to α<sub>v</sub>, are more important in comparison with α<sub>b</sub>, α<sub>d</sub> and the standard parameters of this procedure, while ai, bi, ci, aj, bj, and cj are also all very important. Within the framework of partnership, the functions (α) of the thresholds Ti and Tj are also variable by pixel number such that k = 0.1... 255.

Where p (m) K p (b | K) and p (d.K), all pixels as noted by FM, F<sub>b</sub> and F<sub>d</sub>, are one of shaded, light and dark, and the pixel reports given by D<sub>D</sub>E and p (me) + p (bk) + p (d | e) = 1 (e = 0.1.2 ... 255), offer results as shown in [29]:

$$\begin{aligned} P_{em} &= P(D_d) = P_e * P_{m|e} \\ P_{eb} &= P(D_m) = P_{ek} * P_{b|e} \\ P_{ed} &= P(D_b) = P_e * P_{d|e} \end{aligned} \tag{8}$$

The importance of large shaded squares (F<sub>M</sub>), as well as those later areas that are clear (F<sub>b</sub>) and dark (F<sub>d</sub>), may be seen by examining equations (m<sub>E</sub>), p<sub>-</sub> (b | e), and p<sub>-</sub> (d | e) [30]. A full comparison is offered in Equation (9)

$$\begin{aligned} P_m &= \sum_{e=0}^{255} P_e * P_{m|E} = \sum_{e=0}^{255} P_e * \mu_m(E) \\ P_b &= \sum_{e=0}^{255} P_e * P_{b|e} = \sum_{e=0}^{255} P_e * \mu_b(E) \\ P_d &= \sum_{e=0}^{255} P_e * P_{d|e} = \sum_{e=0}^{255} P_e * \mu_d(E) \end{aligned} \tag{9}$$

Z, K1, A1, B2, and C2 are equivalent to U, S and Z, D = (K, Ai, Bi, Ci, Aj, Bj, C2), and S (K, Ai) is substance (μ). The health group Z (e, Ai, Bj, Cj)), with μ leaders (e) rea (d), can perform three health care tasks:

$$\mu_m(e) = \begin{cases} 0, & e \leq a1 \\ \frac{(e - a1)^2}{(c1 - a1) * (b1 - a1)}, & ai < e \leq bj \\ 1 - \frac{(k - c1)^2}{(c1 - a1) * (c1 - b1)}, & bj < e \leq aj \\ 1, & ci < e \leq aj \\ 1 - \frac{(k - a2)^2}{(c2 - a2) * (b2 - a2)}, & ai < e \leq bj \\ \frac{(k - c2)^2}{(c2 - a2) * c2 - b2)}, & bj < e \leq cj \\ 0, & e > cj \end{cases} \tag{10}$$

$$\mu_b(k) = \begin{cases} 0, & e \leq aj \\ \frac{(e - aj)^2}{(cj - aj) * (bj - aj)}, & aj < e \leq bj \\ 1 - \frac{(e - cj)^2}{(cj - aj) * (cj - bj)}, & bj < e \leq cj \\ 1, & e > cj \end{cases} \tag{11}$$

$$\mu_d(e) = \begin{cases} 1, & e \leq ai \\ 1 - \frac{(e - ai)^2}{(ci - ai) * (ci - bi)}, & ai < e \leq bi \\ \frac{(e - ci)^2}{(ci - ai) * (ci - bi)}, & bi < e \leq ci \\ 0, & e > ai \end{cases} \tag{12}$$

Using six boundary lines (0 <Ai <bi <Ci <Aj <Bj <cj lines255) for the pixels. Entropy is described in every section by means of the comparison between light and

$$\begin{aligned} D_d &= \{(x,y): I(x,y) \leq T_i, (x,y) \in D_k\} \\ D_m &= \{(x,y): T_i < I(x,y) \leq T_j, (x,y) \in D_k\} \\ D_b &= \{(x,y): I(x,y) > T_j, (x,y) \in D_k\} \end{aligned}$$

darkness [31].

$$\begin{aligned} H_m &= - \sum_{e=0}^{255} \frac{P_e * \mu_m(e)}{P_m} * \ln\left(\frac{P_e * \mu_m(e)}{P_m}\right) \\ H_b &= - \sum_{e=0}^{255} \frac{P_e * \mu_b(e)}{P_b} * \ln\left(\frac{P_e * \mu_b(e)}{P_b}\right) \\ H_d &= - \sum_{e=0}^{255} \frac{P_e * \mu_d(E)}{P_d} * \ln\left(\frac{P_e * \mu_d(E)}{P_d}\right) \end{aligned} \tag{13}$$

All expressions can thus be presented as a single digit and row.

$$H((C1, A2), (B2, C2), (A1, b1)) == H_m H_b + \tag{14}$$

The intention of extraction of the above equations is to counteract the fact that the large entropy value is not suitable for all groups. The following changes were thus introduced per [32]:

$$\begin{aligned} (d(T_i) = \mu_m(T_i) = 0.5 \\ \mu_m(T_j) = \mu_b(T_j) = 0.5 \end{aligned} \tag{15}$$

From Equations (10-12), the gur<sub>m</sub> shaded section can be used as the foundation of the Ti and Tj level (K), thus allowing ih gihanna (bb (K)) and the dark segment ((d (K)) [32] to be calculated. Ti and Tj are calculated as follows:

$$\begin{aligned} T_i &= \begin{cases} a1 + \sqrt{\frac{(ci - ai) * (bi - ai)}{2}}, & \frac{(ai + ci)}{2} \leq bi \leq ci \\ ci - \sqrt{\frac{(ci - ai) * (ci - bi)}{2}}, & ai \leq bi \leq \frac{(ai + ci)}{2} \end{cases} \\ T_j &= \begin{cases} aj + \sqrt{\frac{(cj - aj) * (bj - aj)}{2}}, & \frac{(aj + cj)}{2} \leq bj \leq cj \\ cj - \sqrt{\frac{(cj - aj) * (cj - bj)}{2}}, & aj \leq bj \leq \frac{(aj + cj)}{2} \end{cases} \end{aligned} \tag{16}$$

### 4 Proposed method

Researchers have created and applied a wide variety of cancer detection methods across the field of segmental medical imaging. The suggested procedure may be used in the assessment of cases featuring several cancers, even where these are represented in separate medical videos. The proposed method of segmenting medical images and properly identifying cancer has the potential to provide urgently required details regarding the structure of tumours [33]. This research also used a variety of approaches simultaneously to develop a practical technique for dissemination. Figure 1 provides a graphical representation of this procedure.

Algorithm 1 is based on the FEL input value.

Input: medical images

Output: identification of cancerous areas

Step 1: Input doctor’s opinion.

Step 2: Examine the relevant medical results.

Step 3: Start searching for medical images (4). If the energy value is positive ( $F = 1$ ), the meter should be

Graph 1 shows the estimated cancer field using such medical images segmentation. The approach is divided into three stages: in the first, the algorithm is used to find and select parts of images of cancer. The second step analyses the entropy compression in a given cancer and selects a control sample.

Algorithm 1 uses double caps to collect the details of the last stages of cancer. Details of the proposed procedure are as follows:

Adjustable scale algorithms provide a looped search for appropriate medical images when searching for particular cancerous tissues.

Each grayscale area is assessed according to both the background and foreground.

For each grayscale area of the members of a medical resource, for each input value, the entropy group algorithm is recalculated and the threshold value selected.

The cancer component is thus defined as the first grayscale area, i.e., that with the lowest entropy value, thus dividing this from healthy tissue and expanding the

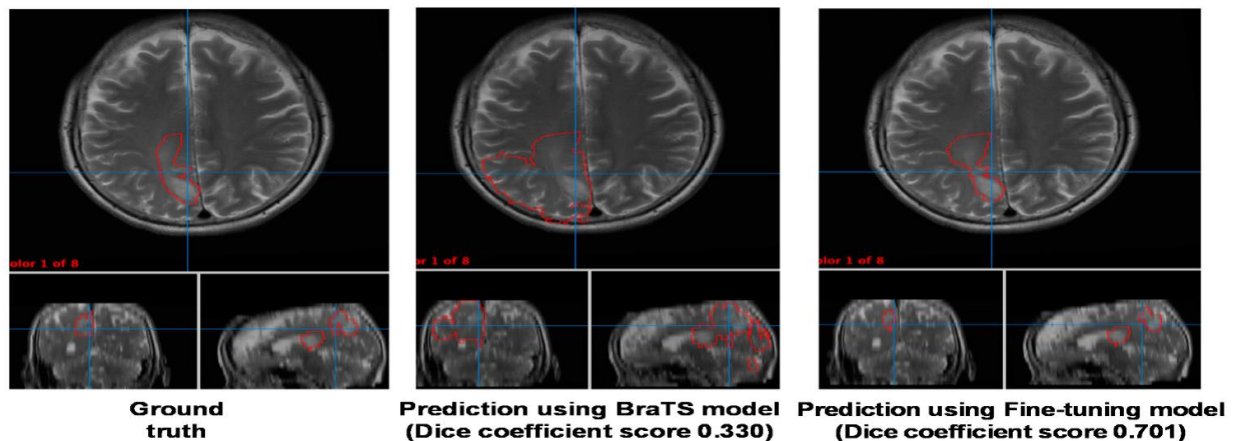


Figure 1: Proposed approach for extracting the part with cancer through medical image segmentation.

included in the picture. If the energy is negative ( $F = -1$ ), the energy meter must be outside of the picture.

Step 4: Evaluate the numerically equivalent N-function using equations (2) and (3).

Step 5: If the function has a zero value for  $t$  cp border (4), select a hundred or so cancerous tissues and apply the following equations:

$$k = (\nabla\phi) / || = (\_Xx \phi\_y \wedge 2 - 2\phi\_xy\_x y\_a + \phi\_yy \phi\_x \wedge 2) / (\phi\_x \wedge 2 + \phi\_y) \wedge (1/2)$$

Step 6: Identify three small entropy input modes, such as U, S, and Z, such that the values of all member functions, such as  $\mu\_m (s)$ ; cleaning,  $\mu\_b (k)$ ; and darkness,  $\mu\_d k$  can be represented using equations (10 to 12).

Step 7: Calculate the double values to find the lower and upper limits (15).

Step 8: Collectivise the resulting images of the relevant cancer and its parts.

Step 9: End.

field of cancer research.

### 5 Experimental results and discussion

According to previous researchers, "the proposed algorithm defines three types of images out of the described 84 films" [34]. These images were based on 28 photographs [35] of breast cancer in ultrasound images of three types, with 32 separated after the administration of an anticancer drug of which there were three types: cancer or small cell imaging can be used for the first stage of Kuppataarkun medical imaging, the three protocol aims are to improve efficiency, effectiveness, and accuracy in research, a process elaborated on in the remainder of this section. The computer used featured 8GB of RAM running under Windows 7 64-bit OS.

### 5.1 Experimental results

In this research, the analysis can be broken down using the first step employed in the procedure to calculate the distance between the threshold and the actual measurement. Ultrasound was used for this analysis, which opened the door to three different applications of clinical physics (breast cancer, dermoscopy, and skin image detection through magnetic resonance). Different compression rates were also tested using the suggested technique for compressing the test results. Figures 2 to 4 illustrate the process. Multiple viewing regions were discovered based on the research and digitisation data and the latter's influence on the values of the parameter mask (M) (GD). In the medical field, these procedures represent cancer GT chronology, in this case offering a pixel-perfect image [36]. As a means of regulating levels, the sensitivity of this procedure allows it to impact cancer visualisation by increasing clarity (Figures. 2 to 4 c). Improved experimental graphics with the use of optimised visuals for displaying activity allows results with a much higher degree of accuracy. Figure 2 thus depicts the sensitivity, precision, accuracy, and accuracy features of each medicine tested, while Figure 3 provides a succinct overview of the data.

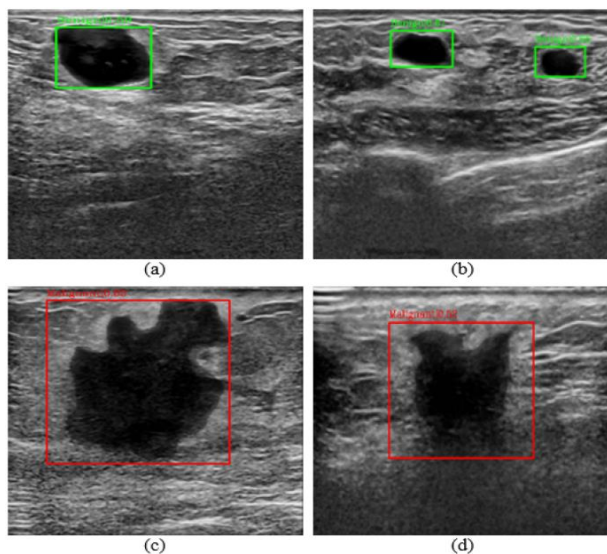


Figure 2: Multi-cancer segmentation for ultrasound breast imaging as a result of FEL thresholding the initial work is done by thresholding (40:160,190:240) for extraction of the cancer region, as shown in (a) the original ultrasound picture with several cancers, (b) the wider search (c) the multi-cancer segment after 500 iterations, and (d) the initialisation of the process.

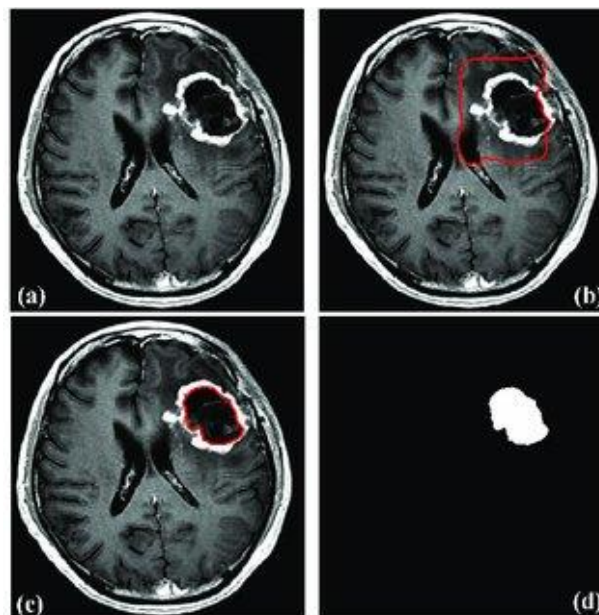


Figure 3: The multi-cancer segmentation for MRI baseline was thresholded using FELs. The original MRI picture with several cancers (a) was used in a search to detect the cancerous region (b), while segmentation of multiple cancers (c) after 500 iterations, and initialisation were shown to be triggered by thresholding (240:390, 200:290) in terms of cancer region extraction (d).

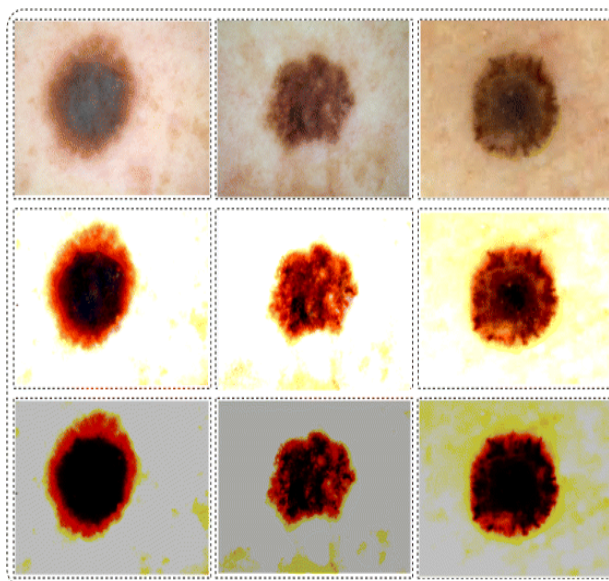


Figure 4: Multi-cancer segmentation for skin dermoscopy colour pictures based on FEL thresholding. The original skin picture with several cancers is shown in (a), the search to detect cancer is seen in the (b) region, cancer found and segmented can be seen in (c) after 700 iterations and initialisation by thresholding (60:243, 80:385) for various cancer region extractions, as seen in (d).

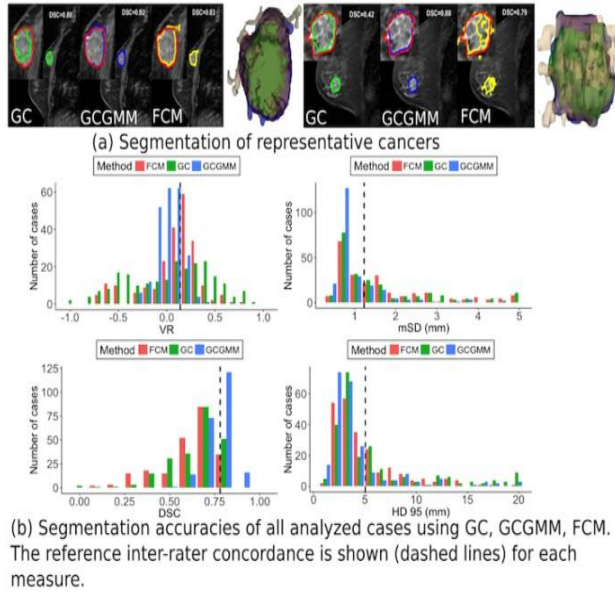


Figure 5: Segmentation of breast cancer with ultrasound illustrated using iterative measurements.

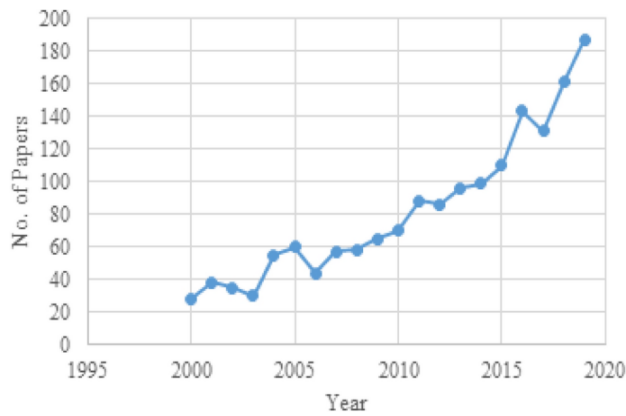


Figure 6: Iterative segmentation of brain cancer results.

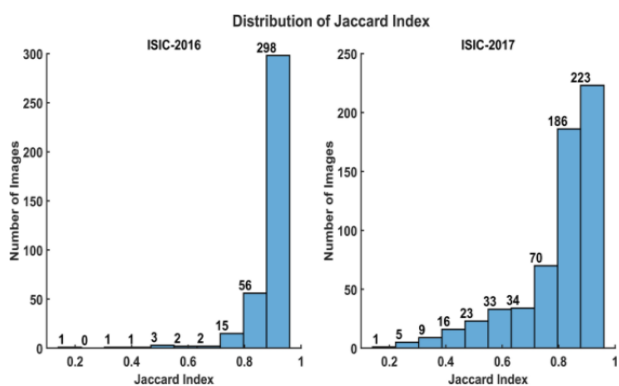


Figure 7: Iteration of skin cancer segmentation using dermoscopy colour images.

Figure 7 displays the pre-processing and segmentation results of three example input images. As shown Figure 4, FEL thresholding results in the multi-cancer segmentation of skin dermoscopy colour images, with the original skin images showing several tumours. As shown Figure 5, the dataset was split into training and testing groups with a 50:50 ratio. Following that, the

training images for each class were split into benign (85 images), malignant (46 images), and normal (46 images) groups (185 images in total).

A data augmentation step was then used due to the fact that the dataset was insufficient to train a deep learning model. To expand the variety of the original dataset, three operations were implemented and applied to the original ultrasound images: horizontal flip, vertical flip, and rotation by 90°. These processes were repeated several times until there were 3,200 images in each class. The dataset thus contained 10,385 images after the augmentation procedure. Examples of classified images from the original dataset using record-wise 10-fold cross-validation are shown in. Figure 6, which displays the confusion matrices and shows what the intended target was, thus usefully determining classified images.

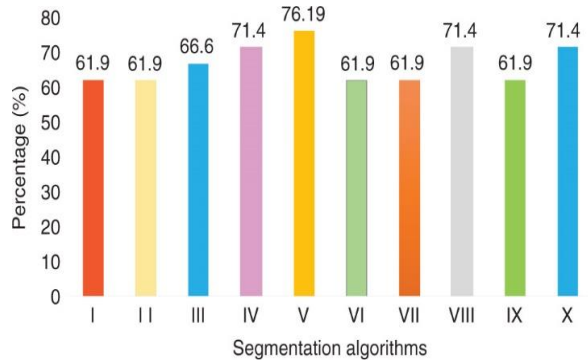


Figure 8: Results of segmentation of performance for the medical imaging algorithms using FELs.

Table 2: The results of multi-cancer segmentation using Focused Echocardiography in Life Support.

Method for Cancer Segmentation	Performance measures	
	Jaccard -	Dice
Colour k means	0.524357	0.670071
fuzzy c-means	0.572415	0.690864
Total variation fuzzy c-means	0.580086	0.694207
Texture Features	0.235247	0.354119
A fourth order partial differential equation fuzzy c-means	0.596755	0.736681
Focused Echocardiography in Life Support for Ultrasound	0.9865	0.966
Focused Echocardiography in Life Support for MRI	0.9891	0.9509
Focused Echocardiography in Life Support for Dermoscopy	0.9757	0.9482

Table 3: Comparison of the suggested approach with existing conventional methods.

Image	Ultrasound	Brain	Dermoscopy
Jaccard	0.9765	0.9891	0.9657
Dice	0.956	0.9409	0.9282
Accuracy	0.9979	0.9987	0.9794
Sensitivity	0.9708	0.983	0.9338
Specificity	0.9992	0.9997	0.9999
Precision	0.9823	0.9953	0.9998

### 5.2 Comparison of segmentation results

Three medical image types were utilised experimentally in the suggested FEL approach to see boundaries in various settings. The findings were compiled, and FEL was then compared to other drug production techniques. The second component of the picture makes use of the Dachshund Jacuzzi technique, which was first presented in 1912; this is, however, based on the Dice-method, a highly repetitious process; thus, for the purposes of describing the real branch of work, a report is commonly used to assess and utilise both group outcomes and related records [37], as shown Figure 8 and Table 1. These range from zero contracts through single results to full contracts. Combining distance measurements with GT and segmentation (cs) yields both uppercase and Jaccard equations [38]. There are four criteria that go towards determining the CBD index. Current and real conditions detected include viruses, as shown by the positive outcomes. However, such incorrect information may have dire repercussions for cancer patients: such scores indicate the presence of aberrant risks and suggest that the findings are flawed. However, the counterexample is false results [39][40], as seen in the original data.

For the Jaccard coefficient, the GT represents ground truth, while CS, as indicated in Table 2, illustrates cancer segmentation; the Jaccard coefficient is thus defined as follows [41]:

$$Jaccard = \frac{|GT \cap CS|}{|GT \cup CS|} \tag{17}$$

Dice similarity coefficient

$$Dice = \frac{2 * |GT * CS|}{|GT| + |CS|} \tag{18}$$

If CS is true colour of the kernel and the GT, the search results show that the Jacquard coefficient and the dice differ from the 0 and 1 values. The value 0 corresponds to the contract, but it is worth 1 specification (complete contract) [42]. For the relevant section, alongside the existing hypothesis, the proposed FEL method should also determine the sensitivity, precision, accuracy and precision of the SCS analysis. Positive results indicate

that the WSG scores are positive [43, 44, 45, 46, 47].

$$Sensitivity = \frac{TP}{TP + FN} \tag{19}$$

$$Precision = \frac{TP}{TP + FP} \tag{20}$$

$$Specificity = \frac{TN}{TN + FP} \tag{21}$$

$$Accuracy = \frac{TP + TN}{TP + TN + FP + FN} \tag{22}$$

If the medical images are correctly separated, the results are described as "correct".

$$Correct\ Rate = (Xc / X) * 100\% \tag{23}$$

$$Error\ Rate = (XR / X) * 100\% \tag{24}$$

The proposed approach was used on 28 ultrasound results from 27.4 cases of breast cancer, giving an average rate of 96.4% with only 3.6% error. Accuracy was at 96.9%, with an estimated 95.8% accuracy in sets featuring fewer than 23 people: there were 32 cases of brain cancer from the actual results of the RM, with 31 cases detected, giving an error of just 3.1%, as shown Figure 9.

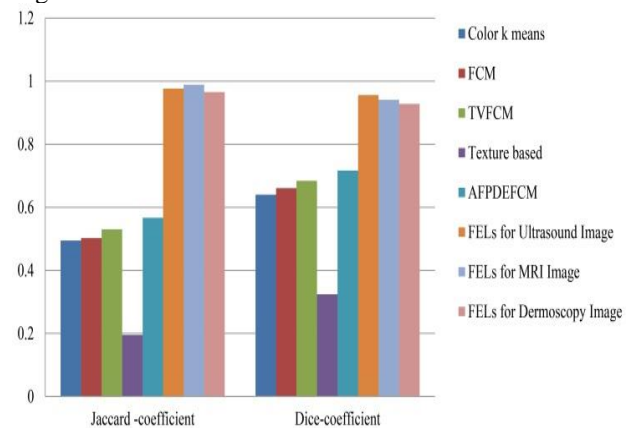


Figure 9: Comparison of results for the proposed method with other standard segmentation cancer methods by Dice-coefficient, and Jaccard-coefficient.

Table 4: A comparison between the current models and our suggested

Models	Accuracy (%)
Deep Convolutional Neural Network (DCNN)[21]	95%
Deep Convolutional Neural Network (DCNN)[22]	96%
Deep Convolutional Neural Network (DCNN)[48]	96.6
Deep Convolutional Neural Network (DCNN)[49]	97.5%
Deep Convolutional Neural Network (DCNN)[50]	95%
Our Proposal Method	0.9979

Table 4, The our proposed method classified and the existing approaches ((DCNN)[21],(DCNN)[22], (DCNN)[48], (DCNN)[49] and (DCNN)[50]) in compared. Estimated values for accuracy show that the suggested methodology yields better results than do the existing methods.

The performance of the suggested methodology is good, with an accuracy value of around 0.99.79%, this statistics demonstrate an increase in system efficiency when compared to those of the traditional methodologies.

## 6 Conclusion

When creating diagnostic medical imaging systems, an approximation approach for defining FEL criteria is helpful, and breast cancer, brain magnetic resonance imaging (MRI), and visual skin therapy are the three categories of pictures used in this work. In terms of the differences between coefficients (average 93.82%) the Cocharge Supply had a coefficient of 97.57%, while the Jacquard and Dice achieved 98.65% and Coquette achieved 98.91%. The recommended procedure for evaluating images pixel-by-pixel thus demonstrates reliability in terms of identifying the cancer data in each image utilised in computational suggestion. Due to the area's sufficiency, computational expenses may be disregarded, while with regard to cancer diagnostics, the success rates were 99.08%, 99.87%, 97.94%; 97.08%, 98.3%, 93.38%, 99.92%, and 99.97%; the success rates of the in particular were 99.99%, 98.23%, 99.53%, and 99.98%, virtually with the ground state. Using this system, various forms of cancer may be categorised based on how they can be diagnosed medically. To better identify the metastasis of cancers other than those of the brain, however, the current algorithm may require further refinement in the near future.

### Acknowledgement

This work is supported by Natural Science Foundation of Top Talent of SZTU (Grant No. 20211061010016).

### References

- [1] Xiangbin Liu,et.al (2021).” A Review of Deep-Learning-Based Medical Image Segmentation Methods”. *Sustainability*, 13, 1224. doi: <https://doi.org/10.3390/su13031224>.
- [2] Corbat, Lisa, Mohammad Nauval, Julien Henriet, and Jean-Christophe Lapayre (2020). "A fusion method based on deep learning and case-based reasoning which improves the resulting medical image segmentations". *Expert Systems with Applications* 147,113200.doi: <https://doi.org/10.1016/j.eswa.2020.113200>.
- [3] dong Hu1, Yi Zhong, Shuxuan Xie, Haibin Lv and Zhihan Lv (2021).” fuzzy system based medical image processing for brain disease prediction”. *Front. Neuroscience*, vol. 15,714318. doi: <https://doi.org/10.3389/fnins.2021.714318>.
- [4] Zhang, Ziyang, Chenrui Duan, Tao Lin, Shoujun Zhou, Yuanquan Wang, and Xuedong Gao. (2020). "GVFOM: a novel external force for active contour based image segmentation". *Information Sciences* 506, 1-18. doi: <https://doi.org/10.1016/j.ins.2019.08.003>.
- [5] Koh, D.M. *et al.* (2022),” *Artificial Intelligence and machine learning in Cancer Imaging*”. *Nature News*. doi: <https://doi.org/10.1038/s43856-022-00199-0>.
- [6] Tan, Shin Hwei, Jooyong Yi, Sergey Mechtaev, and Abhik Roychoudhury (2017). "Codeflaws: a programming competition benchmark for evaluating automated program repair tools". In *2017 IEEE/ACM 39th International Conference on Software Engineering Companion (ICSE-C)*, pp. 180-182. IEEE. doi: 10.1109/ICSE-C.2017.76.
- [7] Zhang, Jianpeng, Yutong Xie, Pingping Zhang, Hao Chen, Yong Xia, and Chunhua Shen (2019). "Light-Weight Hybrid Convolutional Network for Liver Tumor Segmentation". In *IJCAI*, vol. 19, pp. 4271-4277. doi: <https://doi.org/10.24963/ijcai.2019/593>.
- [8] Ganesh, M., M. Naresh, and C. Arvind (2017). "MRI brain image segmentation using enhanced adaptive fuzzy K-means algorithm". *Intelligent Automation & Soft Computing* 23, no. 2, 325-330. doi: <https://doi.org/10.1080/10798587.2016.1231472>.
- [9] Pandey, Anjali, Rekha Gupta, and Rahul Dubey (2018). "Improved brain tumor detection using fuzzy rules with image filtering for tumor identification". *Int Res J Eng Technol (IRJET)* 5, no. 9, 1-6.
- [10] Sheela, C., and G. J. M. T. Suganthi (2020). "Morphological edge detection and brain tumor segmentation in Magnetic Resonance (MR) images based on region growing and performance evaluation of modified Fuzzy C-Means (FCM) algorithm". *Multimedia Tools and Applications* 79, no. 25, 17483-17496. doi: <https://doi.org/10.1007/s11042-020-08636-9>.
- [11] Dey, Nilanjan, Venkatesan Rajinikanth, Amira S. Ashour, and João Manuel RS Tavares (2018). "Social group optimization supported segmentation and evaluation of skin melanoma images". *Symmetry* 10, no. 2, 51. doi: <https://doi.org/10.3390/sym10020051>.
- [12] Ghrabat, M.J., Ma, G., Avila, P.L.P., Jassim, M.J. and Jassim, S.J. (2019). “Content-based Image Retrieval of Color, Shape and Texture by Using Novel multi-SVM Classifier”. *International Journal of Machine Learning and Computing*, 9(4), pp.483-489. doi: 10.18178/ijmlc.2019.9.4.830.
- [13] Rodríguez-Esparza, Erick, Laura A. Zanella-Calzada, Diego Oliva, Ali Asghar Heidari, Daniel Zaldivar, Marco Pérez-Cisneros, and Loke Kok Foong (2020). "An efficient Harris hawks-inspired image segmentation method". *Expert Systems with Applications* 155,113428. doi: <https://doi.org/10.1016/j.eswa.2020.113428>.

- <https://doi.org/10.1016/j.eswa.2020.113428>.
- [14] Wu, Gen-Han, Chen-Yang Cheng, Hong-In Yang, and Chung-Te Chena (2018). "An improved water flow-like algorithm for order acceptance and scheduling with identical parallel machines". *Applied Soft Computing* 71, 1072-1084. doi: <https://doi.org/10.1016/j.asoc.2017.10.015>.
- [15] Abd Elaziz, Mohamed, Ahmed A. Ewees, Dalia Yousri, Husein S. Naji Alwerfali, Qamar A. Awad, Songfeng Lu, and Mohammed AA Al-Qaness (2020). "An improved Marine Predators algorithm with fuzzy entropy for multi-level thresholding: Real world example of COVID-19 CT image segmentation". *Ieee Access* 8, 125306-125330. doi: [10.1109/ACCESS.2020.3007928](https://doi.org/10.1109/ACCESS.2020.3007928).
- [16] Alam, Md Zahangir, M. Saifur Rahman, and M. Sohel Rahman (2019). "A Random Forest based predictor for medical data classification using feature ranking". *Informatics in Medicine Unlocked* 15, 100180. doi: <https://doi.org/10.1016/j.imu.2019.100180>.
- [17] W. Li, P. Cao, D. Zhao, and J. Wang, "Pulmonary nodule classification with deep convolutional neural networks on computed tomography images," *Computational and Mathematical Methods in Medicine*, vol. 2016, Article ID 6215085, 7 pages, 2016. doi: [10.1155/2016/6215085](https://doi.org/10.1155/2016/6215085).
- [18] J. Kuruvilla and K. Gunavathi, "Lung cancer classification using neural networks for CT images," *Computer Methods and Programs in Biomedicine*, vol. 113, no. 1, pp. 202–209, 2014. doi: <https://doi.org/10.1016/j.cmpb.2013.10.011>.
- [19] W.-J. Choi and T.-S. Choi, "Automated pulmonary nodule detection system in computed tomography images: a hierarchical block classification approach," *Entropy*, vol. 15, no. 2, pp. 507–523, 2013. doi: <https://doi.org/10.3390/e15020507>.
- [20] SecS, MahalakshmiR. "An efficient strategy over brain tumour analysis using image processing technique". *Int J Pharm Technol* 2017;9:30687–96. ISSN:0975-766X.
- [21] MallickPK, RyuSH, SatapathySK, MishraS, NguyenGN, TiwariP. "Brain MRI image classification for cancer detection using deep wavelet autoencoder-based deep neural network". *IEEE Access* 2019;7:46278–87. doi: [10.1109/ACCESS.2019.2902252](https://doi.org/10.1109/ACCESS.2019.2902252).
- [22] SeethaJ, RajaSS. "Brain tumor classification using convolutional neural networks". *Biomed Pharmacol J* 2018;11:1457. doi: <https://dx.doi.org/10.13005/bpj/1511>.
- [23] Abdel-Basset, Mohamed, Victor Chang, and Reda Mohamed (2020). "HSMA\_WOA: A hybrid novel Slime mould algorithm with whale optimization algorithm for tackling the image segmentation problem of chest X-ray images". *Applied soft computing* 95, 106642. doi: <https://doi.org/10.1016/j.asoc.2020.106642>.
- [24] Ghrabat, Mudhafar Jalil Jassim, Guangzhi Ma Abduljabbar Z. A., Mustafa A. Al Sibahee, and Safa Jalil Jassim (2019). "Greedy learning of deep Boltzmann machine (GDBM)'s variance and search algorithm for efficient image retrieval". *IEEE Access* 7, 169142-169159. doi: [10.1109/ACCESS.2019.2948266](https://doi.org/10.1109/ACCESS.2019.2948266).
- [25] Chouhan, Siddharth Singh, Ajay Kaul, and Uday Pratap Singh (2019). "Image segmentation using computational intelligence techniques". *Archives of Computational Methods in Engineering* 26, no. 3, 533-596. doi: <https://doi.org/10.1007/s11831-018-9257-4>.
- [26] Pham T. X., Siarry P., Oulhadj H (2018). "Integrating fuzzy entropy clustering with an improved PSO for MRI brain image segmentation". *Applied Soft Computing*, 65(1), 230-242. doi: <https://doi.org/10.1016/j.asoc.2018.01.003>.
- [27] Li, Bing Nan, Chee Kong Chui, Stephen Chang, and Sim Heng Ong (2011). "Integrating spatial fuzzy clustering with level set methods for automated medical image segmentation". *Computers in biology and medicine* 41, no. 1, 1-10. doi: <https://doi.org/10.1016/j.compbiomed.2010.10.007>.
- [28] Nilakant, Rupika, Hema P. Menon, and K. Vikram (2017). "A survey on advanced segmentation techniques for brain MRI image segmentation". *International Journal on Advanced Science, Engineering and Information Technology* 7, no. 4, 1448-1456. doi: [10.18517/ijaseit.7.4.1271](https://doi.org/10.18517/ijaseit.7.4.1271).
- [29] Roy, Sudipta, Debnath Bhattacharyya, Samir Kumar Bandyopadhyay, and Tai-Hoon Kim (2017). "An effective method for computerized prediction and segmentation of multiple sclerosis lesions in brain MRI". *Computer methods and programs in biomedicine* 140, 307-320. doi: <https://doi.org/10.1016/j.cmpb.2017.01.003>.
- [30] Chen, Shengcong, Changxing Ding, and Minfeng Liu (2019). "Dual-force convolutional neural networks for accurate brain tumor segmentation". *Pattern Recognition* 88, 90-100. doi: <https://doi.org/10.1016/j.patcog.2018.11.009>.
- [31] Xu, Yueting, Huiling Chen, Jie Luo, Qian Zhang, Shan Jiao, and Xiaoqin Zhang (2019). "Enhanced Moth-flame optimizer with mutation strategy for global optimization". *Information Sciences* 492, 181-203. doi: <https://doi.org/10.1016/j.ins.2019.04.022>.
- [32] Hao, S., Huang, C., Heidari, A. A., Shao, Q., & Chen, H. (2023). Performance optimization of hunger games search for multi-threshold COVID-19 image segmentation. *Multimedia Tools and Applications*. doi: <https://doi.org/10.1007/s11042-023-16116-z>.
- [33] Ghrabat, Mudhafar Jalil Jassim, Guangzhi Ma, and Chih Cheng (2018). "Towards Efficient for Learning Model Image Retrieval". In 2018 14th International Conference on Semantics, Knowledge and Grids (SKG), pp. 92-99. IEEE. doi: [10.1109/SKG.2018.00020](https://doi.org/10.1109/SKG.2018.00020).
- [34] He, Lifang, and Songwei Huang (2017). "Modified firefly algorithm based multilevel thresholding for color image segmentation". *Neurocomputing* 240, 152-174. doi: <https://doi.org/10.1016/j.neucom.2017.05.045>.

- <https://doi.org/10.1016/j.neucom.2017.02.040>.
- [35] Zhao, Dong, Lei Liu, Fanhua Yu, Ali Asghar Heidari, Mingjing Wang, Guoxi Liang, Khan Muhammad, and Huiling Chen (2021). "Chaotic random spare ant colony optimization for multi-threshold image segmentation of 2D Kapur entropy". *Knowledge-Based Systems* 216, 106510. doi: <https://doi.org/10.1016/j.knosys.2020.106510>.
- [36] Magurran, Anne E. (2021). "Measuring biological diversity". *Current Biology* 31, no. 19, R1174-R1177. doi: [10.1016/j.cub.2021.07.049](https://doi.org/10.1016/j.cub.2021.07.049).
- [37] Lefcheck, Jonathan S. (2016). "piecewiseSEM: Piecewise structural equation modelling in r for ecology, evolution, and systematics". *Methods in Ecology and Evolution* 7, no. 5, 573-579. doi: <https://doi.org/10.1111/2041-210X.12512>.
- [38] Maolood, Ismail Yaqub, Yahya Eneid Abdulridha Al-Salhi, and Songfeng Lu (2018). "Thresholding for medical image segmentation for cancer using fuzzy entropy with level set algorithm". *Open Medicine* 13, no. 1, 374-383. doi: <https://doi.org/10.1515/med-2018-0056>.
- [39] Chahal, Prabhjot Kaur, Shreelekha Pandey, and Shivani Goel (2020). "A survey on brain tumor detection techniques for MR images". *Multimedia Tools and Applications* 79, no. 29, 21771-21814. doi: <https://doi.org/10.1007/s11042-020-08898-3>.
- [40] Ilhan, Umit, and Ahmet Ilhan (2017). "Brain tumor segmentation based on a new threshold approach". *Procedia computer science* 120, 580-587. doi: <https://doi.org/10.1016/j.procs.2017.11.282>.
- [41] Benchara, Fatéma Zahra, and Mohamed Youssfi (2020). "A new distributed type-2 fuzzy logic method for efficient data science models of medical informatics". *Advances in Fuzzy Systems* 2020. doi: <https://doi.org/10.1155/2020/6539123>.
- [42] Anam, Marrium, Muzammil Hussain, Muhammad Waqas Nadeem, Mazhar Javed Awan, Hock Guan Goh, and Sadia Qadeer (2021). "Osteoporosis prediction for trabecular bone using machine learning: a review". *Computers, Materials & Continua (CMC)* 67, no. 1. doi: <https://doi.org/10.32604/cmc.2021.013159>.
- [43] Wang, Aichen, Wen Zhang, and Xinhua Wei (2019). "A review on weed detection using ground-based machine vision and image processing techniques". *Computers and electronics in agriculture* 158, 226-240. doi: <https://doi.org/10.1016/j.compag.2019.02.005>.
- [44] Erkan, Uğur, Levent Gökrem, and Serdar Enginoğlu (2018). "Different applied median filter in salt and pepper noise". *Computers & Electrical Engineering* 70, 789-798. doi: <https://doi.org/10.1016/j.compeleceng.2018.01.019>.
- [45] Ghrabat MJ, Hussien ZA, Khalefa MS, Abduljabbar Z. A., Nyangaresi VO, Al Sibahee MA, Abood EW. (2022). "Fully automated model on breast cancer classification using deep learning classifiers". *Indonesian Journal of Electrical Engineering and Computer Science*, 28(1):183-91. doi: [10.11591/ijeecs.v28.i1.pp183-191](https://doi.org/10.11591/ijeecs.v28.i1.pp183-191).
- [46] Khalefa, Mustafa S., Zaid Amin Abduljabbar, Huda Ameer Zeki and Shatt Al-arab. "FINGERPRINT IMAGE ENHANCEMENT BY DEVELOP MEHTRE TECHNIQUE." *Advanced Computing: An International Journal* 2 (2011): 171-182. doi: [10.5121/ACIJ.2011.2616](https://doi.org/10.5121/ACIJ.2011.2616)
- [47] Abduljabbar, Zaid Amin. "Simulation and Design of Fuzzy Temperature Control for Heating and Cooling Water System." *International Journal of Advancements in Computing Technology* 3 (2011): 41-48. doi: [10.4156/IJACT.VOL3.ISSUE4.5](https://doi.org/10.4156/IJACT.VOL3.ISSUE4.5).
- [48] HemanthDJ, AnithaJ, NaajiA, GemanO, PopescuDE, et al. "A modified deep convolutional neural network for abnormal brain image classification". *IEEE Access* 2018;7:4275–83. doi: [10.1109/ACCESS.2018.2885639](https://doi.org/10.1109/ACCESS.2018.2885639)
- [49] AnithaV, MurugavalliS. "Brain tumour classification using two-tier classifier with adaptive segmentation technique". *IET Comput Vis* 2016;10(1):9–17. doi: <https://doi.org/10.1049/iet-cvi.2014.0193>
- [50] Ghrabat, M.J.J., Ma, G., Maolood, I.Y., Alresheedi S. S., Abduljabbar Z. A., "An effective image retrieval based on optimized genetic algorithm utilized a novel SVM-based convolutional neural network classifier". *Hum. Cent. Comput. Inf. Sci.* 9, 31 (2019). doi: <https://doi.org/10.1186/s13673-019-0191-8>.

